Evolution of neck radius and relaxation of coalescing nanoparticles

David N. McCarthy and Simon A. Brown*
The MacDiarmid Institute for Advanced Materials and Nanotechnology, Department of Physics and Astronomy, University of Canterbury, Private Bag 4800, Christchurch 8140, New Zealand

(Received 18 December 2008; revised manuscript received 26 July 2009; published 13 August 2009)

We use kinetic Monte Carlo simulations to investigate the coalescence of fcc nanoparticles via lattice-based diffusion of surface atoms. The radius of the neck region connecting the two nanoparticles is found to develop with characteristic power laws $r \sim t^a$ with $a \sim \frac{1}{3}$ and $a \sim \frac{1}{6}$ for the early and intermediate stages of coalescence, respectively. For late coalescence stages, when the nucleation of new atomic layers on nanoparticle facets is required for further coalescence, the nanoparticle size, temperature, and nanoparticle orientation all influence the development of the neck. In contrast, classical theory predicts an approximately constant value of $a(\sim\frac{1}{6})$. We also examine the temperature dependence of the equilibration times for relaxing nanoparticles and distinguish the limiting processes to be nucleation of new germs on a facet and/or the detachment of atoms from atomic layers.

DOI: 10.1103/PhysRevB.80.064107 PACS number(s): 61.46.Df, 61.46.Bc

I. INTRODUCTION

Coalescence has been a thoroughly studied field through history due to its importance in numerous situations, from the natural (droplet formation in clouds) to the more applied (sintering of particles for new materials). Coalescence typically occurs via four mass transport modes;[1] surface diffusion, hydrodynamic flow, evaporation-condensation, or volume diffusion. For a pair of spherical particles, each of the four mass transport modes is expected to yield a characteristic power law for the radius of the neck, r, as a function of time, t, of the form $r \propto t^a$.

For two spherical particles coalescing via surface diffusion, Kuczynski[1] predicted the neck radius would develop with $a=\frac{1}{7}$. Later investigations by Mullins and Nichols,[2,3] and Eggers[4] predicted an exponent $a=\frac{1}{6}$. These calculations assumed isotropic surface tension and isotropic surface diffusion, applicable to liquid droplets and continuously curved surfaces. Surface diffusion is expected to be the dominant mass transport mechanism for small particles (less than 1 μm in size[5]) below their bulk melting temperature. Solid nanoparticles are therefore predicted to coalesce via surface diffusion.

Nanoparticle coalescence has been studied using molecular-dynamics (MD) simulations by Lewis *et al.*[6] for three cases: liquid-liquid, liquid-solid, and solid-solid. Lewis *et al.*[6] find the neck radius initially evolves much faster than $t^{1/6}$ because of elastic and plastic deformations not included in earlier numerical studies[1,3,4] but that coalescence slows down at long times due to the presence of facets.

Further MD simulations by Lummen and Kraska[7] found a three-step coalescence process for colliding metal nanoparticles. The first stage occurs very quickly and is related to the initial neck formation at the point of contact. This quickly transforms the nanoparticles into a dumbell shape, which evolves more slowly during the next stage into an ovoid. The final transformation from an ovoid into a sphere is the longest, as the driving force, the difference in surface energy of the two configurations, is very small.

Nanoparticles can, however, form compact structures with surfaces terminated by large facets, invalidating the assumptions of continuous curvature used in the theories of Nichols and Mullins. Using kinetic Monte Carlo (KMC) simulations, Combe *et al.*[8] investigated the equilibration of three-dimensional crystallites as a function of size and temperature. Below the roughening temperature, they show that relaxation is governed by the time scale of nucleation of new germs on a facet. Mullins and Rohrer[9] arrive at similar conclusions and estimate the maximum facet size on which nucleation is appreciable to be ≈ 1 nm. References[8,9] both conclude that the free-energy barrier E_b preventing nucleation of a germ on a bare facet is inversely proportional to the particle's curvature (or proportional to particle size).

Rankin and Sheldon[10,11] showed a unique pathway for the sintering of cubic MgO particles which avoids the nucleation of new germs. MgO (001) facets have a large nucleation barrier E_b but as coalescence progresses, steps from the neck region spread onto the bare (001) facets, providing attachment sites for material from the edges and vertices, and allowing the particles to relax into more spherical shapes. Lewis *et al.*[6] observed a similar result: in one MD simulation the coalescence of two solid nanoparticles produced an extremely small equilibration time due to a favorable initial orientation of the nanoparticles. Therefore the orientation of the two particles plays an important role in coalescence.

No studies of the coalescence kinetics for large (i.e., ≥ 5 nm) nanoparticles have been performed using the KMC technique. In the present work, three variables influencing coalescence via surface diffusion are considered—temperature, nanoparticle size, and nanoparticle orientation. We investigate fcc nanoparticles intersecting at (001), (110), and (111) planes. The major focus of this work is the growth of the neck region connecting the two nanoparticles and the question of what power-law exponent is observed in each situation considered. Diffusion on crystalline surfaces is inherently anisotropic, so we use a KMC algorithm which simulates systems with anisotropic diffusion and compare with the results of Nichols and Mullins,[3] and Eggers,[4] where isotropic diffusion was assumed. We also consider the equilibration times for coalescing nanoparticles, relating the results to classical models of diffusion and nucleation.

II. COMPUTATIONAL DETAILS

A. KMC simulations

The KMC simulations utilize a standard bond counting algorithm[8,12,13] and the computationally efficient event selection method of Schulze.[14] The number of initial neighbors, i, determines the atomic motions, the configuration after the jump having no influence on the diffusion. The activation barrier an atom must overcome in order to move is $E_A = iE_0$, where E_0 is the energy of a single bond. The model—like those of Refs. 8, 12, and 13—does not contain Ehrlich-Schwoebel-type barriers[15] and so it should be considered an approximation to the crystalline particles of interest. The rate p_i at which an atom with i neighbors moves is

$$p_i = \nu \exp(-E_A/k_B T), \tag{1}$$

where $\nu = \frac{k_B T}{h} \approx 10^{13}$ s^{-1} at $T=500$ K. Atoms with many neighbors have smaller rates than atoms with only one or two neighbors, hence they diffuse more slowly. This follows the principle that atoms in regions of positive curvature (i.e., high chemical potential) have fewer bonds and diffuse to regions of negative curvature (lower chemical potential). It is assumed that $E_0 = 0.1$ eV, an average value garnered from calculations of diffusion barriers for the Al(111) surface[16] and used extensively in previous work.[8,12,13]

The rates of different possible events can be influenced by varying the temperature T. For example, from Eq. (1), raising the temperature reduces the difference in the rates of diffusion of an atom with three neighbors relative to that of an atom with four neighbors. Additionally, sweeping the temperature from low to high values activates particular events, e.g., atoms with seven neighbors have negligibly small rates at $T=400$ K, therefore contributing little to the coalescence but are relatively free to move at $T=500$ K. Simulating coalescence at different temperatures allows investigations of kinetic effects which affect the relaxation time scale. For temperatures above 500 K, the increased occurrence of desorption events lead to the loss of material during the simulation, hence an upper bound of $T=500$ K was chosen for the present work.

We simulate pairs of nanoparticles in a constant-temperature environment (as opposed to constant energy coalescence simulations[7,17]), corresponding to situations where nanoparticles are in contact with a noninteracting, thermally conductive substrate such as graphite, or in good thermal contact with a gas. We are interested in the coalescence of nanoparticles on surfaces since it affects the properties of nanoparticle-assembled devices.[18–20]

B. Calculations

For each simulation the pair of nanoparticles is oriented so that the initial neck is formed in a particular crystallographic plane. The atoms in this plane therefore provide a cross section through the neck. The neck radius r is calculated by measuring the mean distance (from the origin) of atoms around the circumference of the neck. Fully relaxed nanoparticle pairs were found to have a radius $\sim 2^{1/3}$ times the original nanoparticle radius, supporting the use of this method.

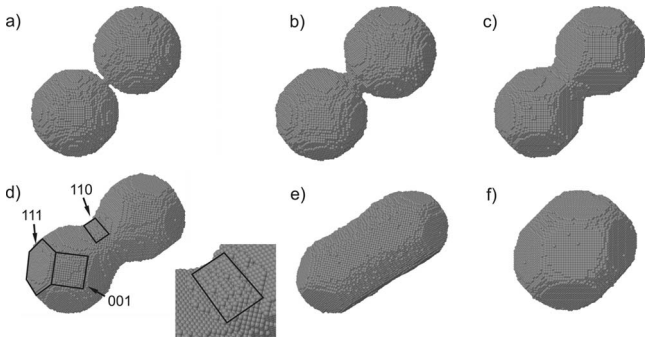

FIG. 1. Six images taken during the coalescence of two $R=14$ nanoparticles intersecting at the (001) plane, with $T=400$ K. Snapshots are taken at (a) $t=1\times10^{-5}$ s, (b) 1×10^{-4} s, (c) 1×10^{-3} s, (d) 4×10^{-3} s with zoomed image of the neck, (e) 5×10^{-2} s, and (f) 8×10^{-1} s.

To quantify the progression of coalescence, the objects' aspect ratios (ARs) are monitored. Comparing the length of the nanoparticle pair, L, with the radius at the neck gives a first approximation to the AR, i.e., $\mathrm{AR} = \frac{L}{r}$. Since the direction of the long axis is normal to the intersection plane, L is defined to be twice the distance separating the atoms furthest along this axis from the origin.

In conjunction with the radius and AR calculations, the total number of bonds $\Sigma_b(t)$ connecting atoms within the object was calculated.[8,13] Reflecting the stochastic nature of KMC simulations, the time t is incremented using $-\frac{\ln(u)}{k}$, where k is the rate constant for shifting out of a state and $\ln(u)$ an exponentially distributed random number.[21] $\Sigma_b(t)$ increases with time as more bonds are formed and reflects a decrease in the total energy of the particle as the surface area decreases.

III. SIMULATIONS AND RESULTS

A. Coalescence of spherical nanoparticles

The first simulations were performed using spherically symmetric nanoparticles, with an initial neck approximately 2 atoms in diameter and the individual nanoparticles ranging in size from 28 000 to 68 000 atoms. Since desorption events are forbidden, the coalesced particle consists of twice the initial number of atoms. Two planes of intersection are considered, the (001) and the (111) cases. In each case the coalescence was monitored for a sufficiently large number of iterations so as to allow the equilibration/relaxation to be complete.

1. (001) intersection plane

Figure 1 shows six stages during the coalescence of a pair of nanoparticles with $R=14$ (the unit of R is the fcc lattice constant). Figure 1(a) is an image soon after the coalescence begins, showing the nanoparticles have reordered from the initial spherical shapes into more faceted objects. Both Figs. 1(a) and 1(b) show the neck region to be highly curved, the neck therefore providing a sink for atoms. In Fig. 1(c) there are few sites of high coordination available at the neck and

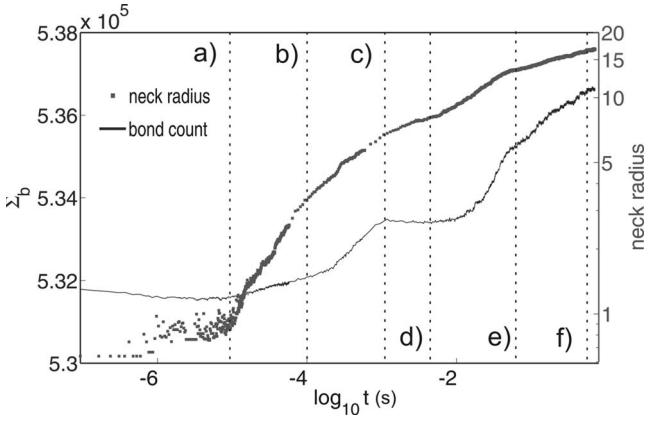

FIG. 2. Plots of the neck radius (square symbols, right-hand scale) and $\Sigma_b(t)$ (full line, left-hand scale) during the coalescence of the nanoparticles shown in Fig. 1. Note the log scales on the horizontal and right-hand axes. Times when snapshots of Fig. 1 were taken are labeled.

attachment to the neck is more difficult. Figure 1(d) shows a rough neck region and the presence of (110) facets around the neck (see inset). Atoms diffuse slowly on (110) planes, allowing them to nucleate new atomic layers with relative ease. From Figs. 1(d) and 1(e), the exposed (110) surfaces at the neck capture material at the expense of the outermost (001) and (111) facets, and the limiting process during this stage is the dissociation of facets (discussed in Sec. III B 1). This process is analogous to the breakup of atomic rows required for the relaxation of vacancy islands in the bidimensional system.[22] Eventually the dumbbell shape is replaced by a faceted rod [Fig. 1(e)], with the circumference made up from alternating (001) and (110) planes. The final growth stages involve a length reduction via the elimination of (001) and (111) facets at the nanoparticle ends, and the corresponding nucleation of new atomic layers on the central region.

Figure 2 shows the neck radius and $\Sigma_b(t)$ data associated with the coalescence depicted in Fig. 1, plotted as functions of time. In Fig. 2 the $\Sigma_b(t)$ data has a linear scale (left-hand axis) while the neck radius is plotted using a log scale (right-hand axis). Time (in seconds) is plotted on the x axis using a log scale and the labels (a)–(f) correspond to the snapshots in Fig. 1. From $t=10^{-6}$ to 10^{-5} s the nanoparticles are reordering, forming facets [see Fig. 1(a)], and little change in $\log[r(t)]$ or $\Sigma_b(t)$ is observed. Between (a) and (c) however, a uniform increase in $\log[r(t)]$ and $\Sigma_b(t)$ is observed, corresponding to the period when the neck region is highly curved [see Figs. 1(a)–1(c)]. From (c) to (d) $\log[r(t)]$ has a shallower slope, reflecting the greater difficulty of attaching atoms around the neck. Additionally from (c) to (d) $\Sigma_b(t)$ is nearly constant since new layers are nucleating only on (110) facets and these layers have higher numbers of unsatisfied bonds than (111) or (001) layers. Between (e) and (f) the slope of $\log[r(t)]$ is shallowest, when the nucleation of atomic layers on (001) facets is required for the nanoparticle to reduce its AR.

Figure 3 shows four plots of the neck radius and $\Sigma_b(t)$ for nanoparticles with $R=12$ and 16, for (001) intersections. In the left-hand column $T=400$ K, in the right-hand column $T=500$ K. For each simulation, coalescence is continued un-

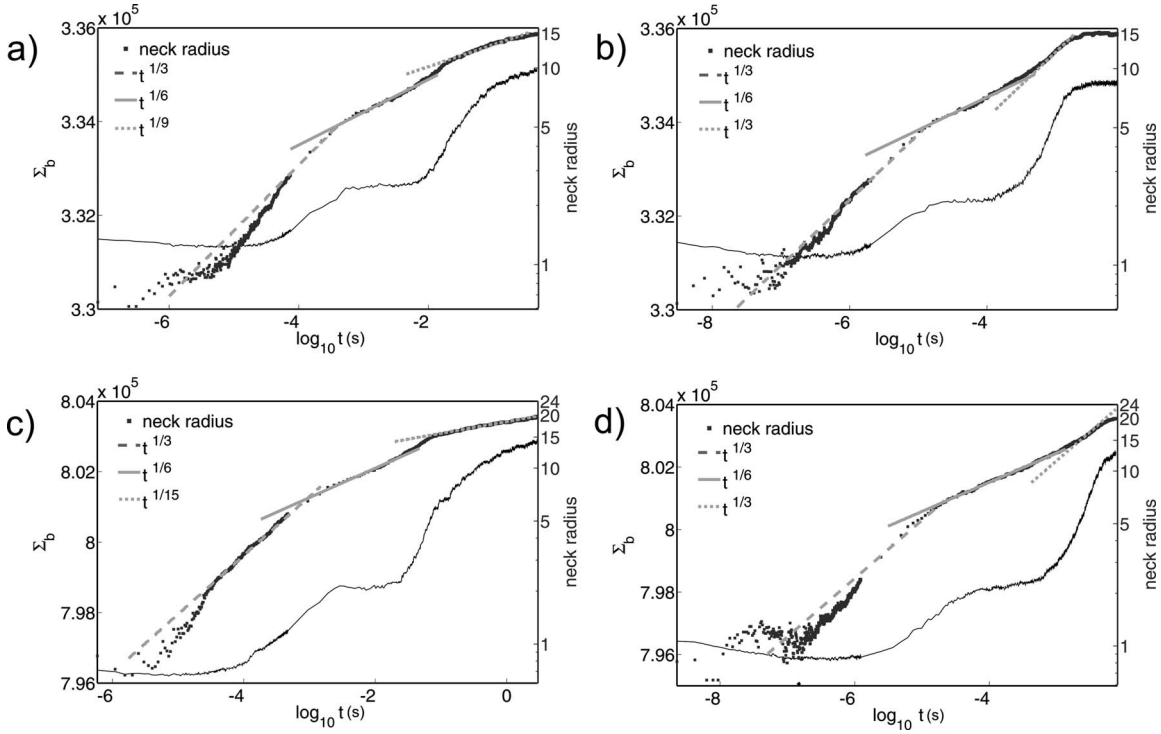

FIG. 3. Plots of neck radius (square symbols, right-hand scale) and $\Sigma_b(t)$ (left-hand scale) for spherical nanoparticles coalescing at the (001) plane. (a) $R=12$, $T=400$ K, (b) $R=12$, $T=500$ K, (c) $R=16$, $T=400$ K, and (d) $R=16$, $T=500$ K. Note the log scales on the horizontal and right-hand axes. The linear regions of $\log[r(t)]$ are fitted assuming a power-law dependence. The legend contains the exponent used to fit the radial data.

til the particles have aspect ratios ~1. Assuming a power-law relationship $r \propto t^a$, lines with slope a are drawn for comparison with each approximately linear region of the $\log[r(t)]$ plot.

In Fig. 3, little variation is apparent between (a) and (c), and between (b) and (d), indicating the nanoparticle size is relatively unimportant. The main point of difference is the time at which the neck radius plateaus, i.e., when the relaxation finishes. Obviously larger nanoparticles require more atoms to travel further in order to reach the most favorable sites and coalescence takes longer (see Sec. III B).

At early stages $a \sim \frac{1}{3}$ and $\log[r(t)]$ and $\Sigma_b(t)$ have no significant temperature dependence. This is because the nanoparticles initially have small facets and contain large numbers of relatively weakly bound atoms, which diffuse/dissociate quickly independent of the temperature. Additionally [as shown in Figs. 1(a) and 1(b)], the neck region is highly curved providing a sink for diffusing atoms. By $r \sim 5$, there is a reduction in curvature at the neck as faceting becomes more prominent and $\log[r(t)]$ begins to track lines with $a \sim \frac{1}{6}$.

During the intermediate stage, where $a \sim \frac{1}{6}$, (110) layers are growing around the neck [see snapshots (c)→(e) of Fig. 1] and there is a plateau in $\Sigma_b(t)$. At the end of the intermediate phase the volume between the two ends of the dumbell is filled in, resulting in strongly faceted structures similar to Fig. 1(e).[23]

The effect of temperature is most apparent when bare (001) and (110) planes are present along the nanoparticle length [see Figs. 1(e) and 1(f)]. At $T=400$ K [Figs. 3(a) and 3(c)], the exponent reduces to $a \sim 1/9$ when $R=12$ and $a \sim 1/15$ when $R=16$. In contrast at $T=500$ K the exponent briefly increases to $a \sim 1/3$ [see Fig. 3(b), $r>10$], before r plateaus at $2^{1/3}R$.

From Figs. 1(e) and 1(f), relaxation of the nanoparticle requires the nucleation of germs on these bare facets. The characteristic time between nucleation events is $\tau_{\text{nucl}} \propto \exp(\frac{E_b}{kT})$.[24] Reducing the temperature to 400 K reduces the rate of nucleation events and the slow nucleation of critically sized germs on (001) planes becomes a significant obstacle to relaxation.

Close inspection of the $\Sigma_b(t)$ data for $T=400$ K ($t>10^{-2}$ s) reveals stepped features which become broader and more numerous for larger sizes [$R=16$ in Fig. 3(c)]. Note that the stepped behavior becomes significant at the same time as $\log[r(t)]$ tracks lines with reduced exponents: $a \sim \frac{1}{9}$ when $R=12$ or $a \sim \frac{1}{15}$ when $R=16$. A similar staircase pattern has been observed previously in Refs. 8 and 13, where each step was interpreted as the nucleation of a new atomic layer. Note that the steps in $\Sigma_b(t)$ represent a decrease in the total energy and should not be confused with the free-energy barrier for nucleation, E_b (see discussion in Refs. 8 and 9).

Figure 4 shows an expanded portion of $\Sigma_b(t)$ data from Fig. 3(c), during the latter stages of coalescence when steps are most obvious. The noisy behavior is due to the nanoparticle switching back and forth between states of differing total energy. In the top left images of Fig. 4, the nucleation of an atomic layer on a (001) surface occurs without the dissociation of any layers. Because the particles shown in Fig. 4

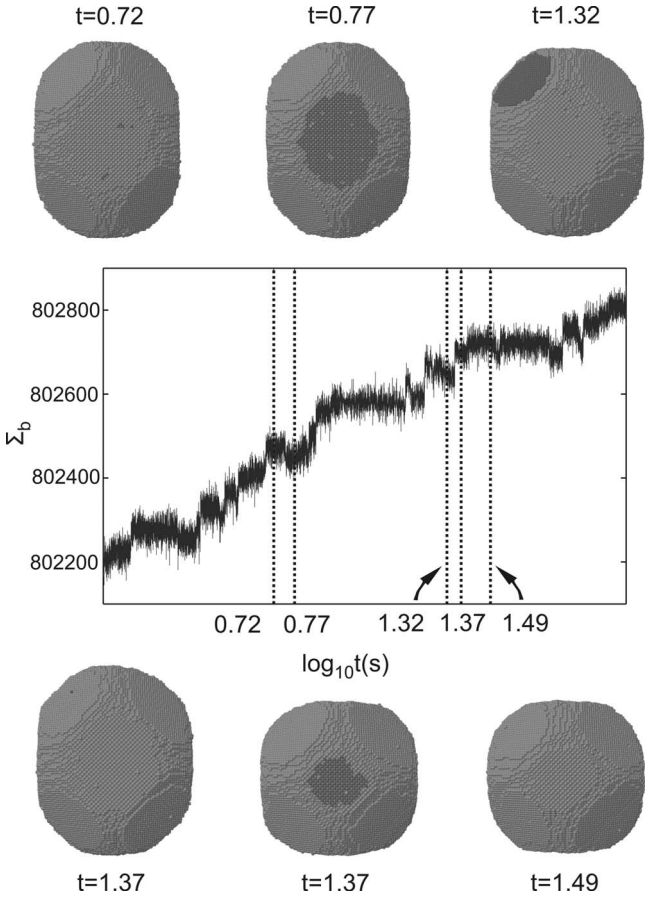

FIG. 4. An expanded view of $\Sigma_b(t)$ showing the staircase behavior. The full data set can be found in Fig. 3(c). The two images at the top left view the nanoparticle from the side, along a (001) plane normal, and show the nucleation of an atomic layer on the (001) plane between $t=0.72$ and 0.77 s. The side-on images at $t=1.32$ and 1.37 s show the dissociation of a (111) oriented atomic layer. The images at bottom right view down the length of the object and show the dissociation of an atomic layer on the (001) plane at the nanoparticle end, between $t=1.37$ and 1.49 s.

have a rough surface, new layers on (001) planes form via material that detachs from edges of nearby (111) planes and as (001) planes have a higher coordination than (111) planes, there is a net decrease in $\Sigma_b(t)$. Between $t=1.32$ and 1.37 s, a layer on a (111) facet dissociates without any new layers nucleating. Dissociated material is incorporated at the edges and vertices of the particle, causing a net reduction in the number of bonds exposed at plane edges and an increase in $\Sigma_b(t)$. The images at the bottom right depict the dissociation of a small layer of (001) atoms from the tip of the object and an increase in $\Sigma_b(t)$.

The staircase in Fig. 4 has separate features associated with the dissociation or the nucleation of atomic layers, whereas Ref. 8 discusses a low-temperature example where particles are highly faceted and dissociation and nucleation occur simultaneously. An examination of the free-energy barriers that limit the dissociation and nucleation of atomic layers is provided in Sec. III B 1. The increase in $\Sigma_b(t)$ in Fig. 4 is similar to the decrease in total energy observed in Ref. 8: from $t=0.72$ to 1.49 s, the particle gradually shifts material

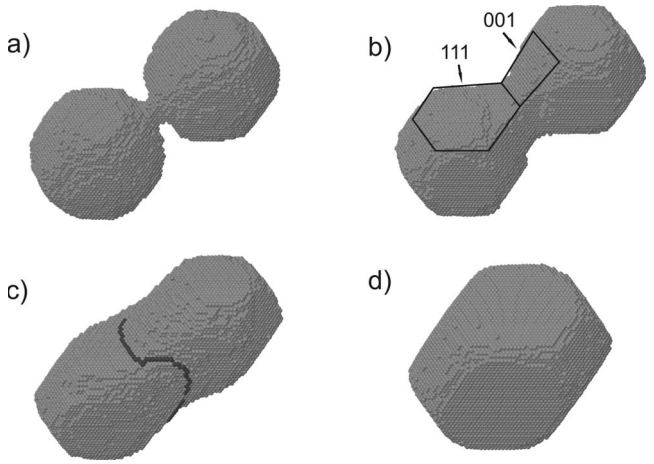

FIG. 5. Four images taken during the coalescence of two $R=14$ nanoparticles intersecting at a (111) plane, with $T=400$ K. Images were taken at (a)$t=1\times10^{-4}$ s, (b) 2×10^{-3} s, (c) 3×10^{-2} s, and (d) 2×10^{-1} s.

from the end planes onto the central planes ($AR_{t=0.72}=1.22$ and $AR_{t=1.49}=1.10$).

2. (111) intersection plane

Simulations were also performed for spherical nanoparticles intersecting at a (111) plane. Figure 5 depicts four stages during the coalescence of two $R=14$ nanoparticles with a (111) intersection, simulated at $T=400$ K. Figure 5(a) shows the nanoparticles soon after the simulation is begun, when small facets have appeared and the neck region remains highly curved. In Fig. 5(b), (001) and (111) facets extend from near the center of each nanoparticle into the apex of the neck so that the neck loses its highly curved nature. At this stage each nanoparticle has three (001) and three (111) planes growing into the neck: the (001) surface planes of one nanoparticle intersect with the (111) surface planes of the opposite nanoparticle. From (b) to (c) atoms diffusing into the neck region are captured at the intersection of (001) and (111) planes. As coalescence progresses new atomic layers spread across the (111) planes, creating a continuous stepped morphology about the neck [see the darker atoms in (c)]. Between (c) and (d), the (111) layers expand further by capturing diffusing atoms at the step edges, increasing the neck radius while reducing the nanoparticle length.

Figure 6 shows the neck radius and $\Sigma_b(t)$ data for $R=14$ nanoparticles coalescing at (a) $T=400$ K and (b) $T=500$ K, with a (111) intersection plane. The data in Fig. 6(a) corresponds to the snapshots in Fig. 5. There are three distinct regions in the $\log[r(t)]$ plots of Fig. 6. Until $r\sim7$, $\log[r(t)]$ develops in a similar manner to nanoparticles coalescing with a (001) intersection, with $a\sim\frac{1}{3}$. The neck region is highly curved in both cases [see Figs. 1(a) and 5(a)], so the lack of a dependence on intersection plane is unsurprising. For intermediate stages, when large facets are present in the neck region, $\log[r(t)]$ is characterized by an exponent $a\sim\frac{1}{6}$ and there is a plateau in $\Sigma_b(t)$. During the "step growth" period [Figs. 5(c) and 5(d)], the slopes of $\log[r(t)]$ and $\Sigma_b(t)$ increase, and $a\sim\frac{1}{3}$ until r plateaus and the relaxation is complete. These three main stages of the radial development ($a\sim\frac{1}{3}, a\sim\frac{1}{6}, a\sim\frac{1}{3}$) all appear in other (111) intersection simulations, irrespective of particle size and temperature [compare Figs. 6(a) and 6(b)].

For both the $T=400$ and 500 K cases, the point at which the neck radius stops increasing is very sharp. This is a significant point of difference to the (001) intersection case, where at low temperatures there is a reduction in a during the latter stages of coalescence, due to the difficulty of nucleating new atomic layers.

The steps in $\Sigma_b(t)$ observed for nanoparticles intersecting at (001) planes (Fig. 4) do not appear for (111) intersections (Fig. 6), even at low temperatures and large nanoparticle sizes. Nucleation of germs is not required during the latter coalescence stages because the step-flow growth of (111) layers, which is a consequence of the initial nanoparticle orientations, allows relaxation via the addition of atoms to existing step edges.

3. Discussion

In the initial stages of coalescence for either intersection case it was found that $a\sim\frac{1}{3}$, changing to $a\sim\frac{1}{6}$ during the middle coalescence stages. Further simulations of spherical or truncated octahedral nanoparticles intersecting at (110) planes also yielded $a\sim\frac{1}{3}$ during early coalescence stages,

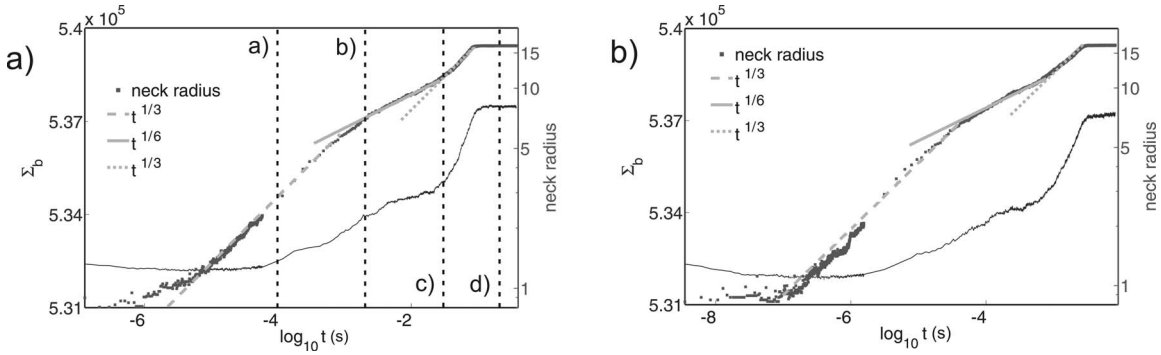

FIG. 6. Development of the neck radius (square symbols, right-hand scale) and $\Sigma_b(t)$ (full line, left-hand scale) for two $R=14$ nanoparticles, intersecting at a (111) plane, coalescing at (a) $T=400$ K and (b) $T=500$ K. Note the log scales on the horizontal and right-hand axes. The lines in (a) correspond to the nanoparticle snapshots in Fig. 5.

suggesting the large exponent at early coalescence stages is not limited to either spherical particles or particular initial geometries.

Nichols and Mullins[3] point out that the power-law exponent a is not constant but ranges from 1/5.9 when $\frac{r}{R} \sim 0.05$ to 1/6.9 at $\frac{r}{R} \sim 0.60$. These values and the exponent $a = \frac{1}{7}$ predicted by Kuczynski[1] and Eggers[4] for continuous surfaces and isotropic diffusion are clearly different to the exponents observed in the present KMC model for spherical particles.

B. Equilibration times of spherical nanoparticles

Macroscopic theories based on surface diffusion predict equilibration times proportional to the fourth power of an object's linear dimension.[3] In this section we analyze the equilibration times for spherical nanoparticles as a function of size and temperature, for both (001) and (111) intersection cases. Equilibration was deemed to have occurred when the AR reached a benchmark value of 1.2,[8] where the nanoparticles have a truncated octahedral shape and the AR changes little with further iterations.

Figure 7(a) is a log-log plot of equilibration times (τ_{eq}), measured from simulations for five different initial nanoparticle sizes at three different temperatures, for both the (001) and (111) intersection cases. Figure 7(a) clearly shows the increase in equilibration times with particle size. The legend shows the temperature for each simulation along with a fitted power-law exponent, b.

Recalling $\tau_{eq} \propto L^4$ from macroscopic theory[3] and making the approximation that $L \sim N^{1/3}$ (where N is the number of atoms in each nanoparticle), the expected scaling behavior is $\tau_{eq} \sim N^b$ with $b = \frac{4}{3}$. Exponents greater than 1.33 indicate that nucleation processes with time scales longer than the time scales associated with surface diffusion are inhibiting the relaxation.[8,9] At $T = 500$ K both intersection cases are well fitted with $b = 1.33$, indicating the coalescence is limited by the rate at which atoms diffuse on the nanoparticle surface. Below $T = 500$ K, the (001) intersection data are fitted with progressively larger exponents, increasing to $b = 2.3$ by $T = 400$ K. The fitted values of b for (111) intersections however show little temperature dependence. The equilibration times for the (001) intersection cases are consistent with the size and temperature dependence observed in Refs. 8 and 13. At high temperature the continuous curvature approximation is valid and $b = 1.33$. At low-temperature particles are strongly faceted and τ_{eq} displays a nonlinear size dependence.

The equilibration times shown in Fig. 7 are consistent with the $r(t)$ data of Figs. 3 and 6. Clearly the difficulty of nucleating new germs at $T = 400$ K for (001) intersections increases the equilibration times and also the value of b. In contrast, the (111) intersections have the expected $b = \frac{4}{3}$ size dependence for each investigated temperature since nucleation is not required for the nanoparticle to move toward an equilibrium structure.

1. Temperature dependence of equilibration times

The temperature dependence of the equilibration times was investigated in more detail for nanoparticles with R

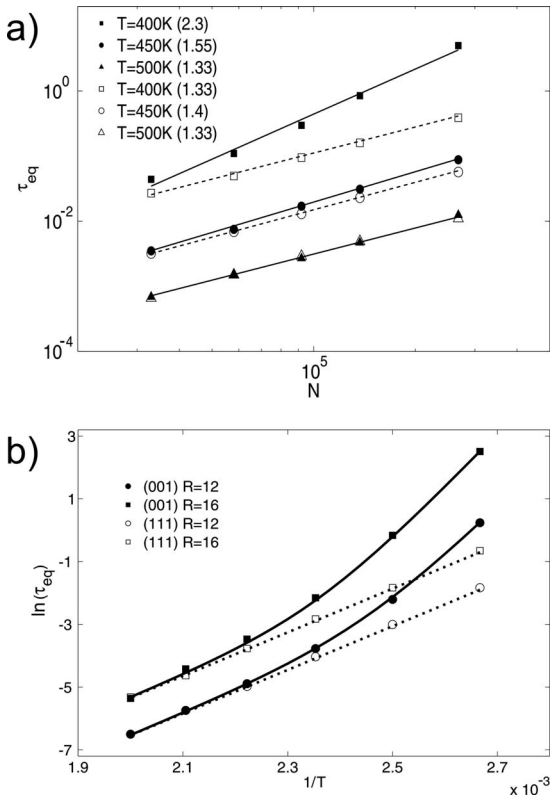

FIG. 7. Equilibration times for the coalescence of spherical nanoparticles intersecting at (001) and 111) planes. (a) Size dependence of the nanoparticle pair equilibration times, for temperatures of $T = 400$, 450, and 500 K, and nanoparticle pairs ranging in size from $N = 33\,000$ to 2 56 000. The filled symbols represent times for (001) intersections while (111) intersections have open symbols. The legend contains the temperatures and slopes of the lines used to fit the data. (b) Arrhenius dependence of the equilibration times. Data from coalescence at (001) intersections is plotted using squares, (111) intersections using circles. Fitted lines are produced using the equations shown in Table I.

$= 12$ and 16 [for both (001) and (111) intersection cases]. The equilibration times are plotted in Fig. 7(b). The data points have been fitted using classical diffusion and nucleation equations (discussed in detail below), and the equations and parameters producing each fit are shown in Table I. Data from (111) intersections show a linear trend while data from (001) intersections curve steeply upward as the temperature is lowered ($\frac{1}{T}$ increases).

For any perfectly faceted configuration, the equilibration process must consist of three steps: dissociation, diffusion, and nucleation. Atoms must first dissociate (detach) from the edges of existing atomic layers, they can then diffuse (both across and between facets) and then nucleate new germs (or join existing germs or steps). It is not obvious, *a priori*, which of these three processes will be the rate-limiting step in the examples considered here.

We first analyze the equilibration times for the relatively simple case of coalesence with a (111) intersection, where nucleation of new germs is clearly unimportant (atoms are always able to join the edges of the steps around the middle of the coalescing pair—see Fig. 5). Both of the dotted lines

TABLE I. Parameters and equations used to fit each data set of Fig. 7.

Fit line	Intersection plane	Radius	Fit
.....	(111)	$R=12$	$1.3\times10^{-9}\exp(\frac{0.6\ \mathrm{eV}}{k_BT})$
.....	(111)	$R=16$	$4.3\times10^{-9}\exp(\frac{0.6\ \mathrm{eV}}{k_BT})$
—	(001)	$R=12$	$1.3\times10^{-9}\exp(\frac{0.6\ \mathrm{eV}}{k_BT})+\frac{2.5\times10^{-18}}{T^{0.5}}\exp(\frac{1.41\ \mathrm{eV}}{k_BT})$
—	(001)	$R=16$	$4.3\times10^{-9}\exp(\frac{0.6\ \mathrm{eV}}{k_BT})+\frac{3.0\times10^{-18}}{T^{0.5}}\exp(\frac{1.48\ \mathrm{eV}}{k_BT})$

in Fig. 7(b) are linear, with a slope which corresponds to an activation energy $E_A=0.6$ eV. Equilibration due to diffusion is governed by the diffusion coefficient, D_s, which has temperature dependence $D_s \propto \exp^{-E_d/k_BT}$, where E_d is the energy barrier for diffusion. A simple bond counting exercise demonstrates that the barriers for diffusion on the low index planes are $E_{d,(111)}=0.3$ eV, $E_{d,(001)}=0.4$ eV, and $E_{d,(110)}=0.5$ eV, all smaller than 0.6 eV, and so the measured activation energy is not simply due to diffusion. Figure 8 gives a closeup view of common layers and neighbor configurations on low index planes: clearly dissociation is initiated by the detachment of atoms from perimeter sites with the smallest binding energy. The compact layers on the low index planes shown in Fig. 8 commonly have sixfold coordinated atoms at their vertices [or chain ends for layers on (110) planes]. Hence the measured activation energy for equilibration times of nanoparticles intersecting at (111) planes corresponds to the energy barrier for detachment of atoms from the layer vertices, 6×0.1 eV$=0.6$ eV.

Our results imply the activation energy associated with the equilibration time is due to a single-particle mechanism, namely, detachment, however, the activation energy can, in principle, result from a collective mechanism. For instance, in Ref. 25 the equilibration of highly faceted particles involves more or less simultaneous detachment, diffusion, and nucleation processes. In the present case the correspondence of $E_A=0.6$ eV with the barrier for detachment from layer vertices is due to the stepped surface morphology [see Fig. 5(c)].

For clusters intersecting at (001) planes we must, in addition to diffusion and dissociation, consider the time scale associated with germ nucleation. A classical expression for the nucleation rate of critical nuclei on *infinite* facets is given by Hirth[26] and Mullins[9] as

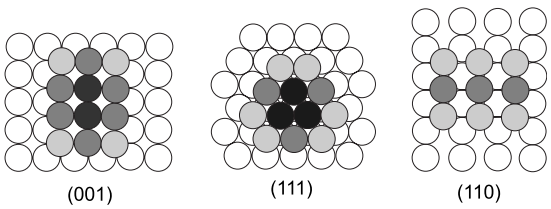

FIG. 8. Compact atomic layers on each of the low index fcc planes. Surface atoms are shaded according to their coordination, substrate atoms are white. Note that the (001) surface atoms have four substrate neighbors, (111) atoms have three, and (110) atoms have five (the fifth atom sitting directly beneath each surface atom).

$$I \propto \frac{D_s}{T^{1/2}}\exp\left(\frac{-E_b}{k_BT}\right), \tag{2}$$

where E_b is the maximum of the free-energy barrier which the system must overcome in order to nucleate a germ on the facets which dominate the nanoparticle length [Fig. 1(e)]. Since Hirth[26] and Mullins[9] do not consider detachment (it is irrelevant on an infinite facet) we believe it is reasonable to assume that, when dissociation dominates the production of free atoms prior to nucleation, E_d can be replaced by E_A yielding $D_s \propto \exp^{-E_A/k_BT}$ and hence

$$I = BT^{1/2}\exp\left(\frac{-E_b-E_A}{k_BT}\right). \tag{3}$$

Now, the total time for all nucleation events to occur, τ_{Nucl}, is the number of nucleation events multiplied by the time required for each nucleation event, $1/I$. Since the number of nucleation events is temperature independent, this leads to

$$\tau_{Nucl} = FT^{-1/2}\exp\left(\frac{E_b+E_A}{k_BT}\right), \tag{4}$$

which includes two free parameters, namely, F which has units [s $K^{1/2}$] and the energy barrier E_b+E_A.

Table I shows the values of F and E_b+E_A found by fitting the (001) intersection data for $R=12$ and 16 in Fig. 7(b). Since the energy barrier limiting detachment of atoms from each of the low index planes is 0.6 eV and is orientation independent [as evidenced by the agreement of the equilibration times for the (001) and (111) intersections at 500 K], we assume that E_A is the same (i.e., $E_A=0.6$ eV) for both intersection cases and so the fitted energies (1.41 and 1.48 eV) lead to nucleation barriers $E_{b,R=12}=0.81$ eV and $E_{b,R=16}=0.88$ eV. The greater value of E_b for larger nanoparticles is in agreement with the expectation that smaller curvatures lead to smaller differences in chemical potential and larger nucleation barriers.[8,9] Combe *et al.*[8] suggest the nucleation barrier is approximately inversely proportional to curvature (equivalently proportional to radius) thus predicting a ratio $\frac{E_{b,R=12}}{E_{b,R=16}}\sim0.75$. We find a ratio of $\frac{0.81}{0.88}\sim0.92$, where the difference is likely due to the lack of continuous curvature for our nanoparticles.

IV. SUMMARY

Irrespective of the nanoparticle size or plane of intersection, in the initial stages of coalescence of spherical nanoparticles it was found that $r \propto t^{1/3}$. Snapshots of the nanoparticles

during early periods (Figs. 1 and 5) show the neck region to be highly curved, providing high coordination sites for material diffusing from the nanoparticle ends. The exponent $a \sim \frac{1}{3}$ is maintained until $r/R \sim 0.3$, at which point well-defined facets intersect at the neck and the nanoparticles each have a faceted dumbell morphology. The dumbell to ovoid phase predicted by Lummen and Kraska is characterized by an exponent $a \sim \frac{1}{6}$. Finally, during the late stages of coalescence the exponent can range from $a \sim \frac{1}{15}$ (when relaxation is prevented by a large nucleation barrier) to $a \sim \frac{1}{3}$ (when the nucleation barrier is negligible).

The comparisons of τ_{eq} for each intersection case illustrate the importance of particle orientation on coalescence. For high temperatures, or favorable intersections, the equilibration times for the KMC model agreed with predictions assuming isotropic diffusion. In such cases, our results find the time scale for coalescence is determined by the energy barrier limiting the detachment of atoms from atomic layers, i.e., 0.6 eV for layers on low index planes. At low temperatures, and unfavorable intersections, relaxation occurs only if the nucleation of new islands is possible.

ACKNOWLEDGMENTS

The authors would like to thank Timothy Schulze for providing the framework of the bond counting code and Shaun Hendy for useful discussions and coding expertise.

*simon.brown@canterbury.ac.nz

[1] G. Kuczynski, J. Appl. Phys. **20**, 1160 (1949).
[2] W. W. Mullins, J. Appl. Phys. **30**, 77 (1959).
[3] F. Nichols and W. Mullins, J. Appl. Phys. **36**, 1826 (1965).
[4] J. Eggers, Phys. Rev. Lett. **80**, 2634 (1998).
[5] W. Mullins, J. Appl. Phys. **28**, 333 (1957).
[6] L. J. Lewis, P. Jensen, and J.-L. Barrat, Phys. Rev. B **56**, 2248 (1997).
[7] N. Lummen and T. Kraska, Phys. Rev. B **71**, 205403 (2005).
[8] N. Combe, P. Jensen, and A. Pimpinelli, Phys. Rev. Lett. **85**, 110 (2000).
[9] W. Mullins and G. Rohrer, J. Am. Ceram. Soc. **83**, 214 (2000).
[10] J. Rankin and B. W. Sheldon, J. Am. Ceram. Soc. **82**, 1868 (1999).
[11] B. W. Sheldon and J. Rankin, J. Am. Ceram. Soc. **82**, 1873 (1999).
[12] P. Jensen and N. Combe, Comput. Mater. Sci. **24**, 78 (2002).
[13] A. La Magna, Surf. Sci. **601**, 308 (2007).
[14] T. P. Schulze, Phys. Rev. E **65**, 036704 (2002).
[15] R. L. Schwoebel and E. J. Shipsey, J. Appl. Phys. **37**, 3682 (1966).
[16] A. Bogicevic, J. Strömquist, and B. I. Lundqvist, Phys. Rev. Lett. **81**, 637 (1998).
[17] S. Hendy, S. A. Brown, and M. Hyslop, Phys. Rev. B **68**, 241403(R) (2003).
[18] R. Reichel *et al.*, Appl. Phys. Lett. **89**, 213105 (2006).
[19] J. van Lith, A. Lassesson, S. A. Brown, M. Schulze, J. G. Partridge, and A. Ayesh, Appl. Phys. Lett. **91**, 181910 (2007).
[20] A. Lassesson, M. Schulze, J. van Lith, and S. A. Brown, Nanotechnology **19**, 015502 (2008).
[21] A. F. Voter, Phys. Rev. B **34**, 6819 (1986).
[22] J. L. Iguain and L. J. Lewis, Phys. Rev. B **68**, 195407 (2003).
[23] We note that for simulations of particles with (110) intersections, the early stage $a \sim \frac{1}{3}$ and intermediate stage $a \sim \frac{1}{6}$ slopes are also observed but once an elongated faceted structure similar to Fig. 1(e) is reached, the structure cannot equilibrate further due to the relatively low temperature of our simulations.
[24] A. Pimpinelli and J. Villain, *Physics of Crystal Growth* (Cambridge University Press, Cambridge, England, 1998).
[25] N. Combe and H. Larralde, Phys. Rev. B **62**, 16074 (2000).
[26] J. P. Hirth, Acta Metall. **7**, 755 (1959).